ACS Catalysis

UF University of Florida Libraries

Subscriber access provided by University of Florida | Smathers Libraries

Article

Supported Palladium–Gold Alloy Catalysts for Efficient and Selective Hydrosilylation under Mild Conditions; Isolated Single Palladium Atoms in Alloy Nanoparticles as the Main Active Site

Hiroki Miura, Keisuke Endo, Ryoichi Ogawa, and Tetsuya Shishido

ACS Catal., **Just Accepted Manuscript** • DOI: 10.1021/acscatal.6b02767 • Publication Date (Web): 17 Jan 2017

Downloaded from http://pubs.acs.org on January 17, 2017

Just Accepted

"Just Accepted" manuscripts have been peer-reviewed and accepted for publication. They are posted online prior to technical editing, formatting for publication and author proofing. The American Chemical Society provides "Just Accepted" as a free service to the research community to expedite the dissemination of scientific material as soon as possible after acceptance. "Just Accepted" manuscripts appear in full in PDF format accompanied by an HTML abstract. "Just Accepted" manuscripts have been fully peer reviewed, but should not be considered the official version of record. They are accessible to all readers and citable by the Digital Object Identifier (DOI®). "Just Accepted" is an optional service offered to authors. Therefore, the "Just Accepted" Web site may not include all articles that will be published in the journal. After a manuscript is technically edited and formatted, it will be removed from the "Just Accepted" Web site and published as an ASAP article. Note that technical editing may introduce minor changes to the manuscript text and/or graphics which could affect content, and all legal disclaimers and ethical guidelines that apply to the journal pertain. ACS cannot be held responsible for errors or consequences arising from the use of information contained in these "Just Accepted" manuscripts.

ACS Publications

ACS Catalysis is published by the American Chemical Society. 1155 Sixteenth Street N.W., Washington, DC 20036

Published by American Chemical Society. Copyright © American Chemical Society. However, no copyright claim is made to original U.S. Government works, or works produced by employees of any Commonwealth realm Crown government in the course of their duties.

Supported Palladium–Gold Alloy Catalysts for Efficient and Selective Hydrosilylation under Mild Conditions; Isolated Single Palladium Atoms in Alloy Nanoparticles as the Main Active Site

Hiroki Miura[a,b,c], Keisuke Endo[a], Ryoichi Ogawa[a], Tetsuya Shishido[a,b,c*]

[a] Department of Applied Chemistry, Graduate School of Urban Environmental Sciences, Tokyo Metropolitan University, 1-1 Minami-Osawa, Hachioji, Tokyo 192-0397, Japan

[b] Research Center for Hydrogen Energy-based Society, Tokyo Metropolitan University, 1-1 Minami-Osawa, Hachioji, Tokyo 192-0397, Japan

[c] Elements Strategy Initiative for Catalysts & Batteries, Kyoto University, Katsura, Nishikyo-ku, Kyoto 615-8520, Japan

* Corresponding author: Tel: +81-42-677-2850, Fax: +81-42-677-2850 (T. Shishido)

E-mail address: shishido-tetsuya@tmu.ac.jp (T. Shishido)

Abstract

Supported Pd–Au alloy catalysts were developed for the highly efficient and selective hydrosilylation of α,β-unsaturated ketones and alkynes. The Pd/Au atomic ratio of the Pd–Au alloy and the supporting material affected the catalytic activity, and supported Pd–Au alloy nanoparticles with a low Pd/Au atomic ratio functioned as highly active heterogeneous catalysts under mild reaction conditions. Structural characterization of supported Pd–Au alloy catalysts by X-ray diffraction (XRD), X-ray absorption spectroscopy (XAS) and transmission electron microscopy (TEM) revealed the formation of random Pd–Au alloy nanoparticles with a uniform size of around 3 nm on the support. Furthermore, XAS and X-ray photoelectron spectroscopy (XPS) elucidated the charge-transfer from Pd to Au and the formation of isolated single Pd atoms in random Pd–Au alloys with a low Pd/Au ratio, which enabled the efficient hydrosilylation of a variety of substrates under mild reaction conditions.

Keywords

Hydrosilylation, heterogeneous catalysts, Pd–Au alloy, silyl enol ether, vinylsilane, X-ray absorption spectroscopy

1. Introduction

Hydrosilylation of unsaturated organic compounds is the most straightforward and atom-economical method for synthesizing organosilicon molecules,[1–3] which are widely used as important synthetic intermediates in the fields of organic chemistry and medicinal chemistry as well as in polymer science. To achieve efficient and economical hydrosilylation, highly active catalytic systems that use transition-metals are needed.[4–9] Furthermore, the current demand for green transformations of organic molecules enhances the importance of heterogeneous catalysts that can facilitate the recycling of precious metals and help to prevent contamination of the products by toxic metals.[10–20] Among a series of heterogeneous catalysts, metal nanoparticles (NPs) and their immobilized variants have been extensively investigated and are considered to be promising tools for the realization of environmentally benign organic transformations.[21–23] To date, monometallic NPs composed of Pt,[24–28] Pd,[29–32] Rh,[33–34] Ni,[35] and Au[36–40] have been used as efficient catalysts for the hydrosilylation of unsaturated organic compounds. However, the reactions have often been carried out at elevated temperatures since they show lower activities than homogeneous catalysts. Thus, the development of a novel catalytic system that can operate at ambient temperature would be very important with regard to both synthetic and green chemistry. On the other hand, considerable attention has recently been focused on the catalysis of alloy NPs in the field of synthetic chemistry.[41–44] Alloy NPs, which are composed of two or more kinds of metals, may exhibit unique catalytic functions due to their completely different electronic states and structural conformations compared to the original monometallic NPs (ligand and ensemble effects). For instance, Pd–Au alloy NPs can provide certain catalytic functions in organic syntheses,[45–48] and Pd–Au alloy catalysts have been shown to offer superior catalytic activities in the oxidation of alcohols,[49–51] polyols[52–55] and hydrocarbons.[56,57] Sakurai et al. developed the Pd–Au bimetallic nanocluster-catalyzed efficient Ullman coupling of aryl chlorides under mild reaction conditions, whereas monometallic Pd or Au NPs showed no

activity.[58–61] Very recently, Yamamoto and Jin et al. reported the 1,4-hydrosilylation of cyclic *α*,*β*-unsaturated ketones with the use of nanoporous Pd–Au alloy as a heterogeneous catalyst to provide the corresponding silyl enol ethers.[62,63] However, elevated temperatures were required to obtain the products in satisfactory yields, and the successful substrates were limited to cyclic enones. Hence, novel catalytic systems that can be applied to the reactions of both cyclic and acyclic *α*,*β*-unsaturated ketones under mild reaction conditions are still needed. Furthermore, the correlations of the structure and electronic states with the activity of Pd–Au alloy catalysts have not been fully clarified.

Herein, we describe the development of highly active supported Pd–Au alloy catalysts for the hydrosilylation of *α*,*β*-unsaturated ketones as well as internal alkynes. The atomic ratio of Pd/Au and the supports for the catalysts remarkably affected their catalytic activities. The detailed characterization of supported Pd–Au catalysts by a series of spectroscopic techniques revealed the formation of isolated single Pd atoms surrounded by Au atoms in a random Pd–Au alloy with a low Pd/Au atomic ratio, which realized the highly efficient selective hydrosilylation of various unsaturated compounds under mild reaction conditions.

2. Results and discussion

2.1 Catalytic performance of supported Pd–Au alloy catalysts for the hydrosilylation of an *α,β*-unsaturated ketone.

The hydrosilylation of *α,β*-unsaturated carbonyl compounds provides the corresponding silyl enol ethers, which are widely used as important substrates in organic synthetic reactions such as Mukaiyama-aldol condensations.[64–76] The reactions of an acyclic *α,β*-unsaturated ketone (**1a)** with triethylsilane (**2a**) in the presence of SiO_2-supported Pd or Au monometallic catalysts at 75 ^oC gave the corresponding silyl enol ether **3a** in very low yields (Table 1, entries 1 and 2). In contrast, supported Pd–Au alloy catalysts gave **3a** (Table 1, entries 3–8), and supported 1Pd3Au/SiO_2 showed the highest activity among the SiO_2-supported catalysts (Table 1, entry 6). Notably, the product was obtained with high *Z*-selectivity. In reactions with homogeneous metal complex catalysts, the stereoselectivity of the products is generally controlled with the aid of phosphine ligands.[75] In contrast, the present supported Pd–Au catalysts did not require the addition of organic ligands to realize highly stereoselective reactions. Furthermore, the reactions proceeded chemoselectively, and products resulting from the 1,2-hydrosilylation of **1a** were not obtained at all. Subsequently, the effect of the support on the catalytic activity of 1Pd3Au alloy nanoparticles was investigated. The reaction at room temperature with catalysts supported on SiO_2, Al_2O_3 and CeO_2 resulted in low yields of **3a** (Table 1, entries 9–11). On the other hand, ZrO_2- and TiO_2- supported catalysts showed moderate to good activities (Table 1, entries 12 and 13), and the product **3a** was obtained in the highest yield with Nb_2O_5-supported catalysts. With these results in mind, we again surveyed the optimal Pd/Au ratio for Nb_2O_5-supported catalysts (Table 1, entries 14–19). As a result, Nb_2O_5-supported 1Pd5Au alloy showed the highest activity, and **3a** was obtained in a total yield of 85% after the reaction had proceeded for 1 h at room temperature. Neither the support nor the Pd/Au atomic ratio influenced the *E*/*Z* selectivities of the products.

Table 1. Optimization of the catalyst

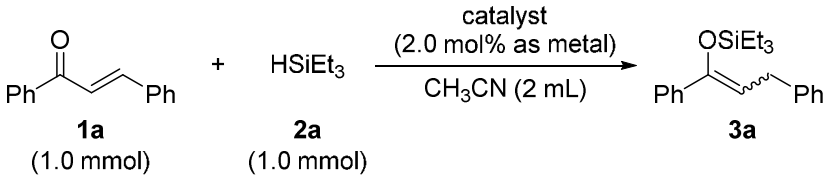

1a (1.0 mmol) **2a** (1.0 mmol) **3a**

entry	catalyst	temp. / °C	time	yield (%)[a]	
				3a	*Z/E*
1	Pd/SiO_2	75	20 min	0	-
2	Au/SiO_2	75	20 min	5	99 : 1
3	$3Pd1Au/SiO_2$	75	20 min	0	-
4	$1Pd1Au/SiO_2$	75	20 min	3	89 : 11
5	$1Pd2Au/SiO_2$	75	20 min	38	92 : 2
6	$1Pd3Au/SiO_2$	75	20 min	59	94 : 6
7	$1Pd5Au/SiO_2$	75	20 min	18	94 : 6
8	$1Pd10Au/SiO_2$	75	20 min	10	93 : 7
9	$1Pd3Au/SiO_2$	r.t.	3 h	4	93 : 7
10	$1Pd3Au/Al_2O_3$	r.t.	3 h	1	-
11	$1Pd3Au/CeO_2$	r.t.	3 h	6	94 : 6
12	$1Pd3Au/ZrO_2$	r.t.	3 h	13	93 : 7
13	$1Pd3Au/TiO_2$	r.t.	3 h	24	93 : 7
14	$1Pd3Au/Nb_2O_5$	r.t.	3 h	45	92 : 8
15	$1Pd5Au/Nb_2O_5$	r.t.	1 h	85	93 : 7
16	$1Pd10Au/Nb_2O_5$	r.t.	3 h	63	93 : 7
17	Au/Nb_2O_5	r.t.	3 h	1	-
18	Pd/Nb_2O_5	r.t.	3 h	0	-

[a]Determined by GLC.

A series of silyl enol ethers were synthesized through the hydrosilylation of unsaturated ketones with 1Pd5Au/Nb_2O_5 catalysts under mild conditions (Table 2). The reactions of a wide range of substituted chalcones with triethylsilane proceeded smoothly to give the corresponding silyl enol ethers (**3b**–**3i**) in good to high yields with excellent *Z*-selectivity. A silyl enol ether bearing a furan ring (**3j**) was obtained in satisfactory yield. Alkyl-substituted *α*,*β*-unsaturated ketone could also be used in the present catalytic system to furnish **3k** in good yield. The reactions of an *α*,*β*-unsaturated aldehyde and methyl ketones provided the corresponding products (**3l**–**3n**) in high yields, while a low *Z*/*E* regioselective reaction and 1,2-hydrosilylation were observed as undesirable side reactions. The reaction of cyclic ketones gave the corresponding silyl enolates (**3o** and **3p**) in good yield. Although longer reaction times and elevated temperatures were required, the reactions of chalcone with hydrosilanes other than triethylsilane gave the corresponding products (**3q**–**3s**) in high yields.

Table 2. Scope of substrates[a]

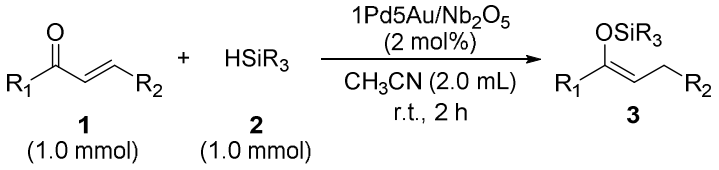

1 (1.0 mmol) **2** (1.0 mmol) **3**

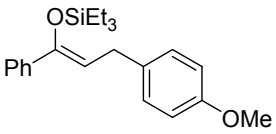

3b 67% (94 : 6)

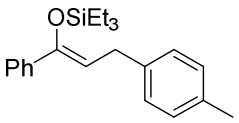

3c 65% (94 : 6)

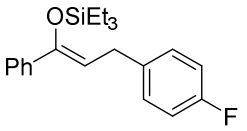

3d 80% (96 : 4)

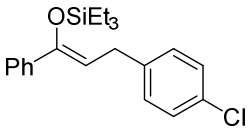

3e 72% (96 : 4)

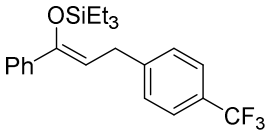

3f 80%[b] (95 : 5)

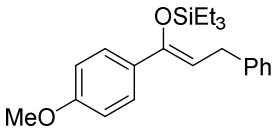

3g 64%[c] (99 : 1)

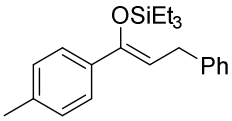

3h 59% (94 : 6)

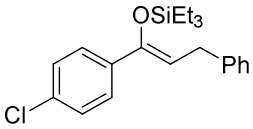

3i 69% (95 : 5)

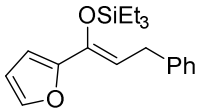

3j 54%[c] (90 : 10)

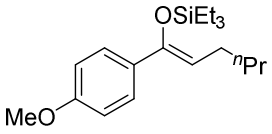

3k 68% (93 : 7)

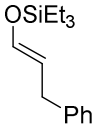

3l 75%[b,d] (0 : 100)

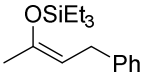

3m 80%[b,e] (36 : 64)

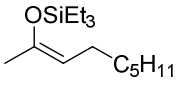

3n 77% (32 : 68)

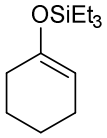

3o 68%

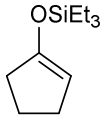

3p 66%

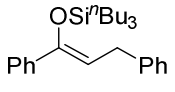

3q 76%[f] (95 : 5)

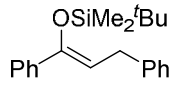

3r 81%[g] (92 : 8)

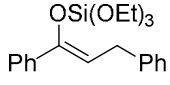

3s 46%[b,g] (99 : 1)

[a] Isolated yields. Values in parentheses show the *Z*:*E* ratio determined by ^{1}H NMR. [b] Yield was determined by ^{1}H NMR using mesitylene as an internal standard. [c] Reaction for 3 h. [d] 1,4-addition/1,2-addition=33/67. [e] 1,4-addition /1,2-addition =65/35. [f] Reaction for 5 h. [g] Reaction at 75 °C, for 8 h.

The supported Pd–Au alloy catalysts were also useful in the hydrosilylation of alkynes to give vinylsilanes, which are versatile and valuable organosilicon compounds in organic synthesis. Careful screening of the supported catalysts also demonstrated that 1Pd5Au/Nb_2O_5 was a useful catalyst for the hydrosilylation of alkynes.[77] Table 3 shows the results of the reactions of a variety of internal alkynes with hydrosilanes under mild conditions; the corresponding vinylsilanes were obtained in high yields. Several examples of the heterogeneous Pt-, Pd-, Rh- or Au-catalyzed hydrosilylation of internal alkynes have been developed so far. We describe here the first example of such reactions at ambient temperature. All of the products in the present alkyne hydrosilylation were obtained with complete *trans* configurations.

Table 3. Hydrosilylation of internal alkynes by PdAu/Nb_2O_5[a]

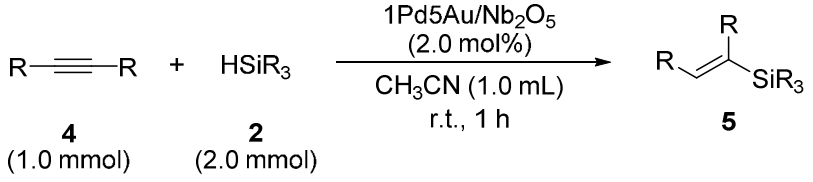

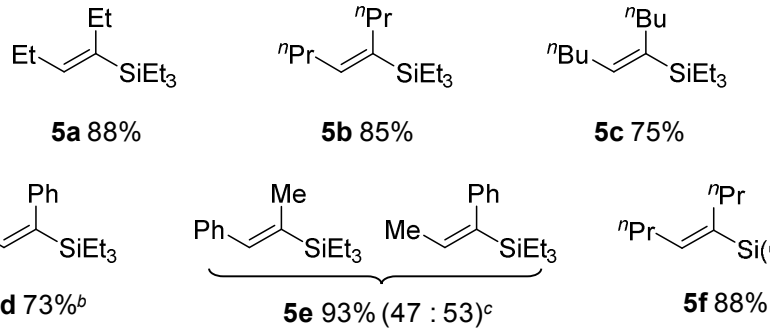

[a] Isolated yield. [b] Reaction at 40 °C for 3 h. [c] Regioselectivity was determined by ^{1}H NMR.

2.2 Characterization of supported Pd–Au alloy catalysts

To understand the remarkable effects of the Pd/Au ratio on the catalytic activities in the hydrosilylation of α,β-unsaturated ketones, the structural and electronic states of supported Pd–Au alloy catalysts were characterized by a series of spectroscopic techniques. Although Nb_2O_5-supported catalysts showed the highest activity, the following discussions on the effect of the Pd/Au ratio on catalytic activity are based on the characterization results for SiO_2-supported catalysts. As described later, this is because some of the characterization data for Nb_2O_5-supported catalysts could not provide sufficient information about the structure and electronic state of Pd–Au NPs due to the detection limits.

Figure 1 shows the XRD patterns of SiO_2-supported Pd–Au alloy catalysts with different Pd/Au ratios. In the patterns of SiO_2-supported Pd or Au monometallic catalysts, the diffraction peaks due to Au(111) and Pd(111) appeared at 2θ = 38.3 and 40.1 (ICDD PDF-2; Au: No.00-004-0784 and Pd: No.00-005-0681), respectively. In the spectra of Pd–Au alloy catalysts, the peaks appeared between the two original peaks, and shifted to a lower angle with a decrease in the Pd/Au atomic ratio. Figure 2 shows a plot of the lattice parameters of Pd–Au alloy NPs estimated from the XRD diffraction pattern of (111) phases as a function of the amount of Au in Pd–Au NPs as determined by atomic absorption analysis.[78] The dashed line in Figure 2 shows the theoretical relationship between the lattice constant and the Pd/Au ratio given by Vegard's law.[79] The lattice parameter increased as the Au content in the alloy NPs increased, and the plot closely follow the dashed line. These results indicate that the two different metals in the NPs are homogeneously mixed to form random alloys. On the other hand, in the patterns of Al_2O_3-, CeO_2-, ZrO_2-, TiO_2- and Nb_2O_5-supported catalysts, distinct peaks attributed to 1Pd3Au NPs and Pd–Au NPs with different Pd/Au ratios were not identified due to the formation of small alloy NPs (Figures S1 and S2 in SI).

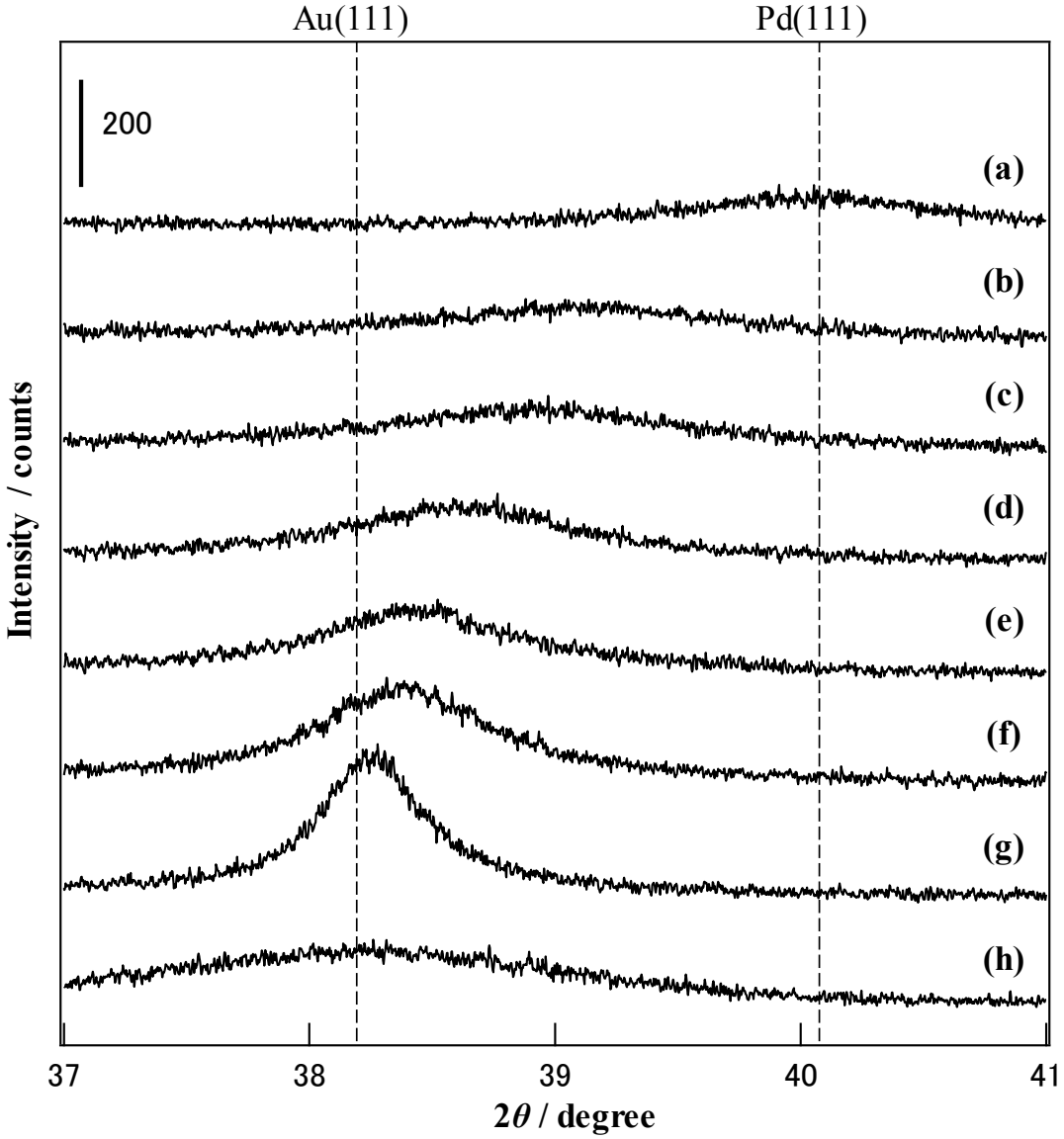

Figure 1. XRD patterns of SiO_2-supported PdAu alloy catalysts with different Pd/Au ratios (a)Pd only, (b)3Pd1Au, (c)1Pd1Au, (d)1Pd2Au, (e)1Pd3Au, (f)1Pd5Au, (g)1Pd10Au, (h)Au only

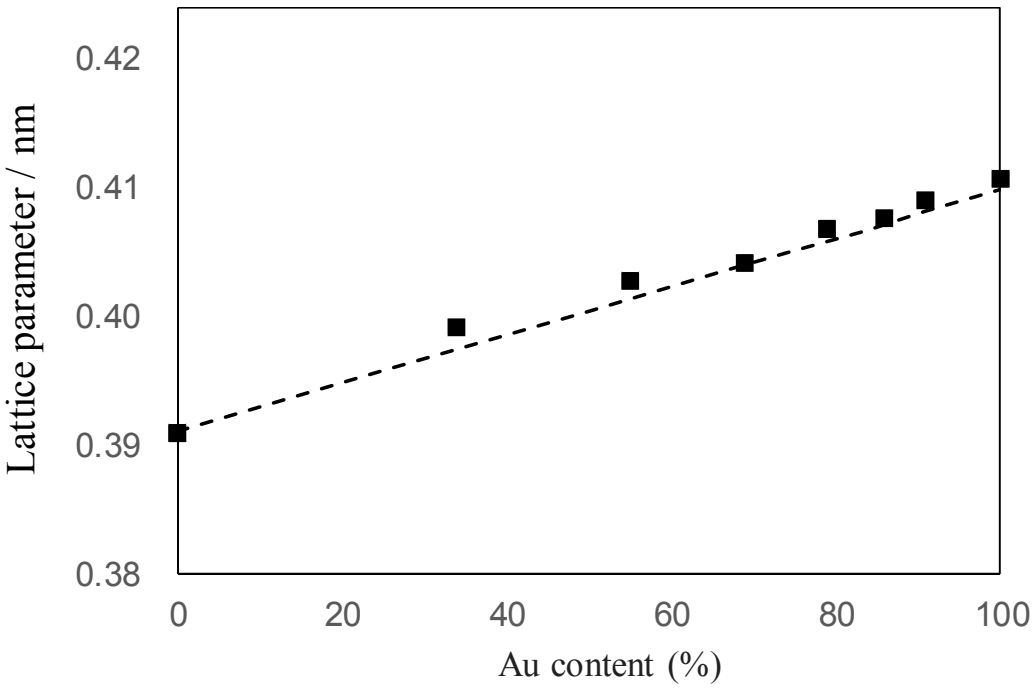

Figure 2. Dependence of the lattice parameters of PdAu alloys on the relative amount of Au.

The morphologies of Pd–Au alloy NPs were identified by TEM observation. HAADF-STEM images and the size distribution histograms for SiO_2- or Nb_2O_5-supported Pd–Au alloy catalysts with a series of Pd/Au ratios are shown in Figures 3 and 4. Figure 5 shows those of 1Pd3Au alloy catalysts on various supports. Although a small fraction of PdAu NPs with large diameter (>10 nm) in the NPs with low Pd/Au ratios were observed, well-dispersed Pu–Au alloy NPs with a diameter of *ca*. 3 nm were found to be mainly present on the surface of each support and noteworthy differences in the mean diameter were not observed. This strongly suggests that remarkable differences in the catalytic activities for hydrosilylation were mainly dominated by the factor other than the differences in the particle size of the alloy NPs.

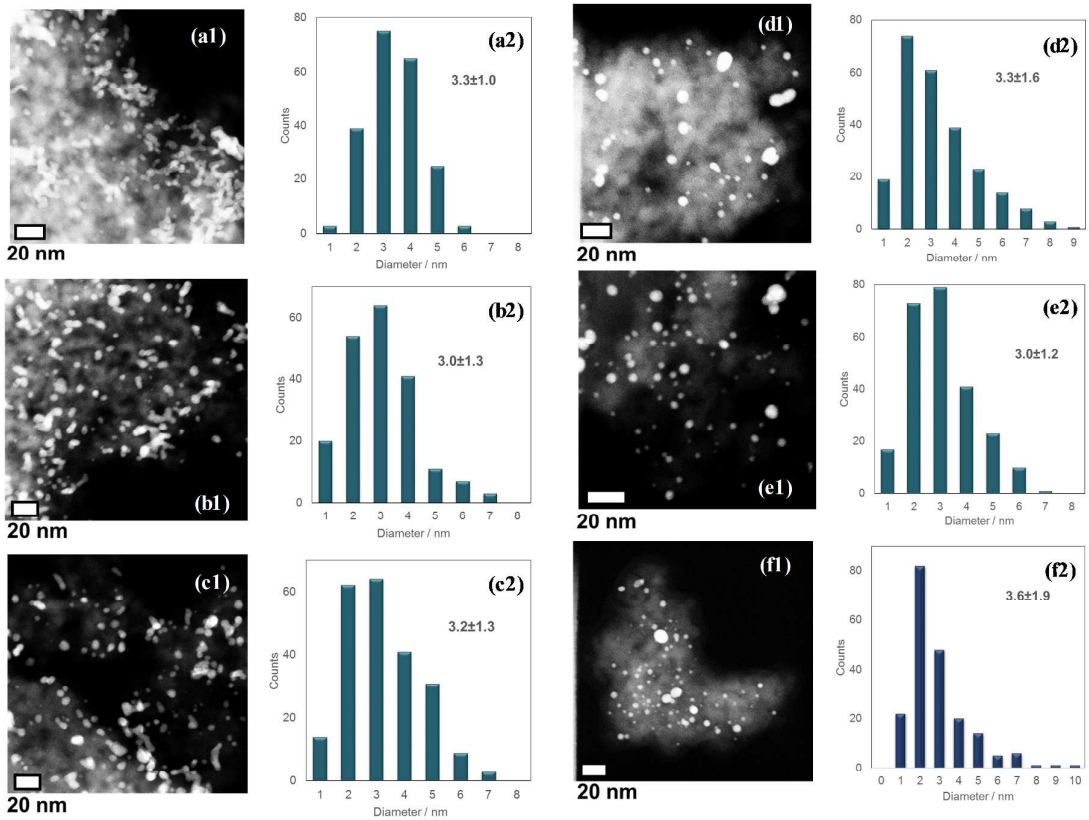

Figure 3. HAADF-STEM images of SiO_2-supported PdAu alloy catalysts with different Pd/Au ratios (a1)3Pd1Au, (b1)1Pd1Au, (c1)1Pd2Au, (d1)1Pd3Au, (e1)1Pd5Au, (f1)1Pd10Au, and (a2–f2) their particle size distribution histograms.

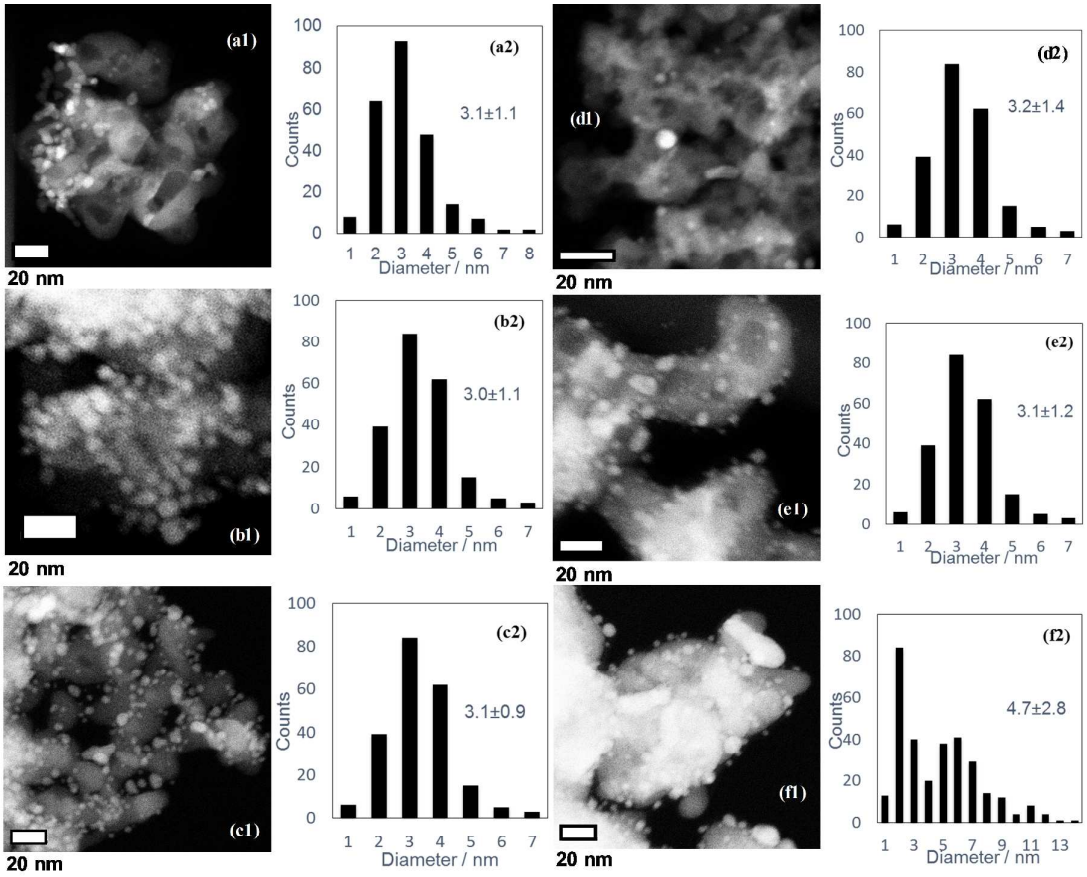

Figure 4. HAADF-STEM images of Nb_2O_5-supported PdAu alloy catalysts with different Pd/Au ratios (a1)3Pd1Au, (b1)1Pd1Au, (c1)1Pd2Au, (d1)1Pd3Au, (e1)1Pd5Au, (f1)1Pd10Au, and (a2–f2) their particle size distribution histograms.

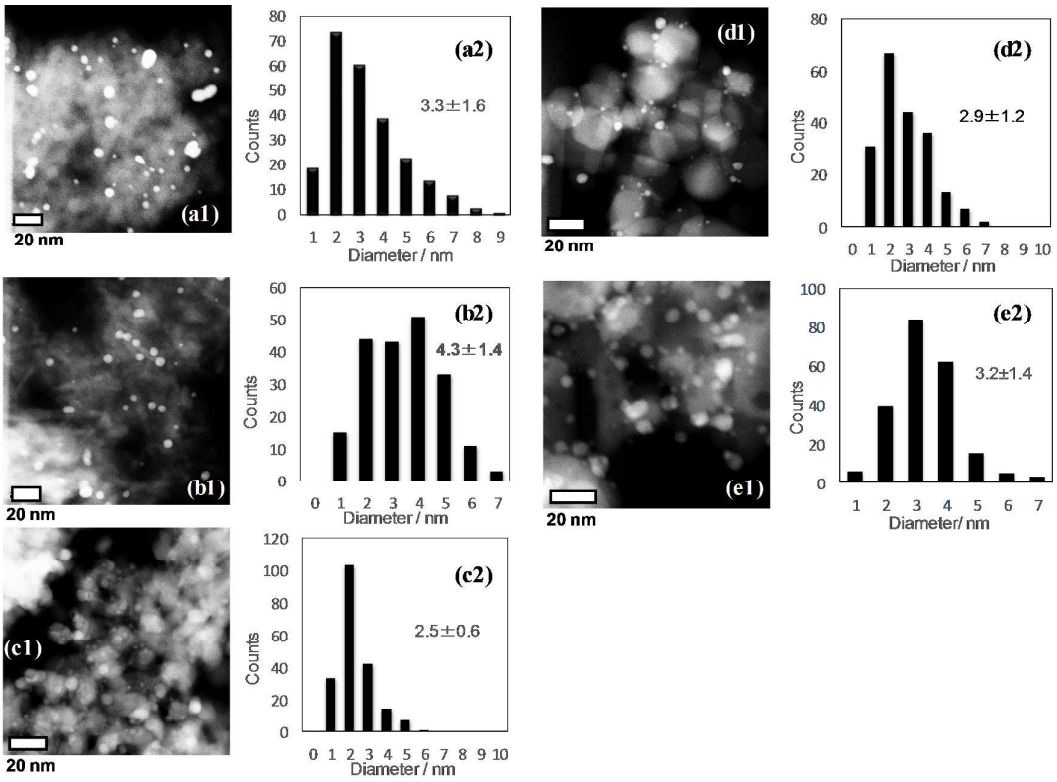

Figure 5. HAADF-STEM images of supported PdAu alloy catalysts on (a1)SiO_2, (b1)Al_2O_3, (c1)ZrO_2, (d1)TiO_2, (e1)Nb_2O_5, and (a2–e2) their particle size distribution histograms.

To evaluate the electronic state of supported Pd–Au alloy catalysts, XPS measurements were carried out. Figure 6 shows the XP spectra of SiO_2-supported Pd–Au catalysts with a series of Pd/Au atomic ratios. In the spectrum of 1Pd10Au/SiO_2, the peaks due to Au $4f_{7/2}$ and $4f_{5/2}$ appeared at 84.1 eV and 87.6 eV, respectively. On the other hand, the peaks of other Pd–Au alloy catalysts were shifted to a lower binding energy with an increase in the Pd/Au ratio. This clearly indicated that electron transfer from Pd atoms to Au atoms occurs when these elements form an alloy. This electron transfer is consistent with the Pauling electronegativity of Au (2.54) relative to Pd (2.20). On the other hand, the peaks ascribed to Pd $3d_{5/2}$ and $3d_{3/2}$ generally appear at around 335 eV and 340 eV, respectively.[80] In the present cases, however, these were too difficult to analyze due to their low intensity and overlapping of the peaks attributed to Au $4d_{5/2}$ (Figure S3 in SI). Similar phenomena were observed in the spectra of Nb_2O_5-supported Pd–Au alloy catalysts with a variety of Pd/Au atomic ratios (Figures S4 and S5 in SI).

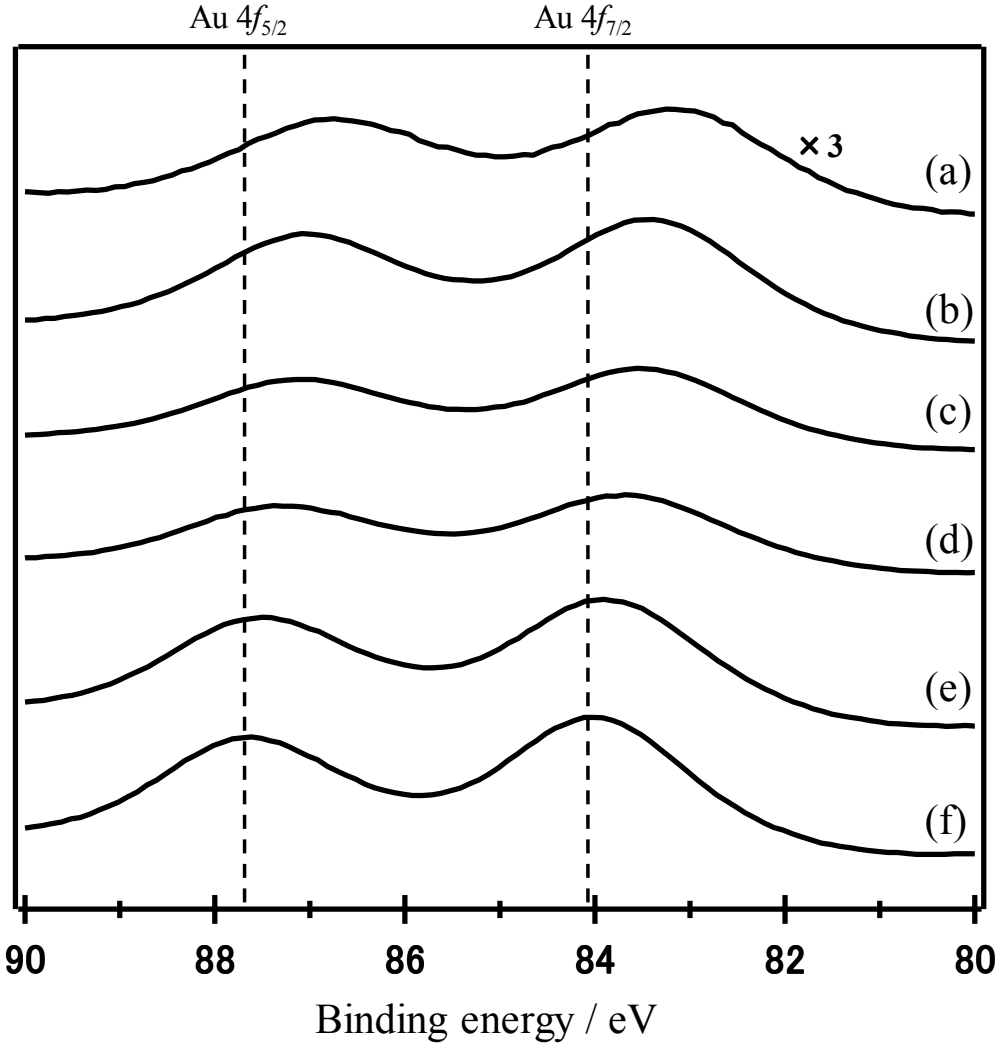

Figure 6. XP spectra around the Au 4f states of SiO_2-supported PdAu alloy catalysts with different Pd/Au ratios (a)3Pd1Au, (b)1Pd1Au, (c)1Pd2Au, (d)1Pd3Au, (e)1Pd5Au, (f) 1Pd10Au.

To gain further insight into the local structures and electronic states of Pd–Au alloy NPs on supports, a series of catalysts were characterized by XAS. Normalized Au L_3-edge XANES spectra of SiO_2-supported Pd–Au alloy catalysts and Au foil are shown in Figure 7. The shape and absorption edge energy of the spectra of supported Pd–Au alloy catalysts with different Pd/Au ratios are very close to those of Au foil, which suggests that the Au in alloy NPs is present as metallic states. On the other hand, the white-line intensities of supported Pd–Au alloy catalysts appeared at 11921 eV, which is lower than that for Au foil. Furthermore, the height of the white-line decreased with an increase in the Pd/Au ratio in alloy NPs. The Au L_3-edge X-ray absorption white-lines correspond to electronic transitions from the $2p_{3/2}$ core-level state and directly reflect the electronic states of the vacant *d* orbitals of Au.[81] The intensity of the Au L_3 X-ray absorption spectrum is related to the *d*-electron valences, and the low intensity of the white-line indicates the presence of electron-rich Au species. These results clearly indicate that charge-transfer from Pd to Au occurs by alloying of Pd and Au. These results are completely consistent with the results of XPS analysis. Pd K-edge XANES spectra of SiO_2-supported Pd–Au alloy catalysts are shown in Figure 8. Regardless of the Pd/Au molar ratio, Pd K-edge XANES spectra shows the presence of metallic Pd species. Generally, the electronic states of Pd species can be evaluated by the E_0 values in XANES spectra. However, energy shifts in E_0 values of a series of PdAu catalysts was unclear. This is probably due to lower energy resolution at Pd K-edge (24 .4 keV) than that at Au L_3-egde (11.9 keV). We are now investigating the Pd-L_3 edge XANES spectra of a series of PdAu catalysts with different PdAu ratio to evaluate their electronic states of the vacant *d* orbitals of Pd species in PdAu alloys.

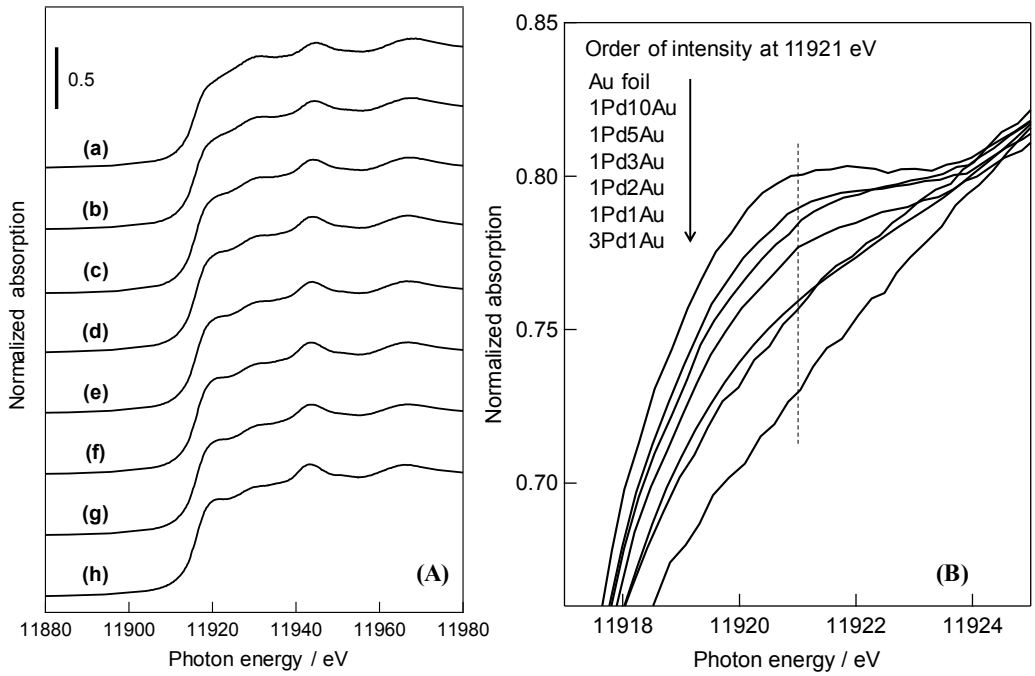

Figure 7. Au L_3-edge XANES spectra (A) and their magnification around the white-line (B) of SiO_2-supported PdAu alloy catalysts with different Pd/Au ratios (a)3Pd1Au, (b)1Pd1Au, (c)1Pd2Au, (d)1Pd3Au, (e)1Pd5Au, (f) 1Pd10Au, (g)Au only, and (h) Au foil.

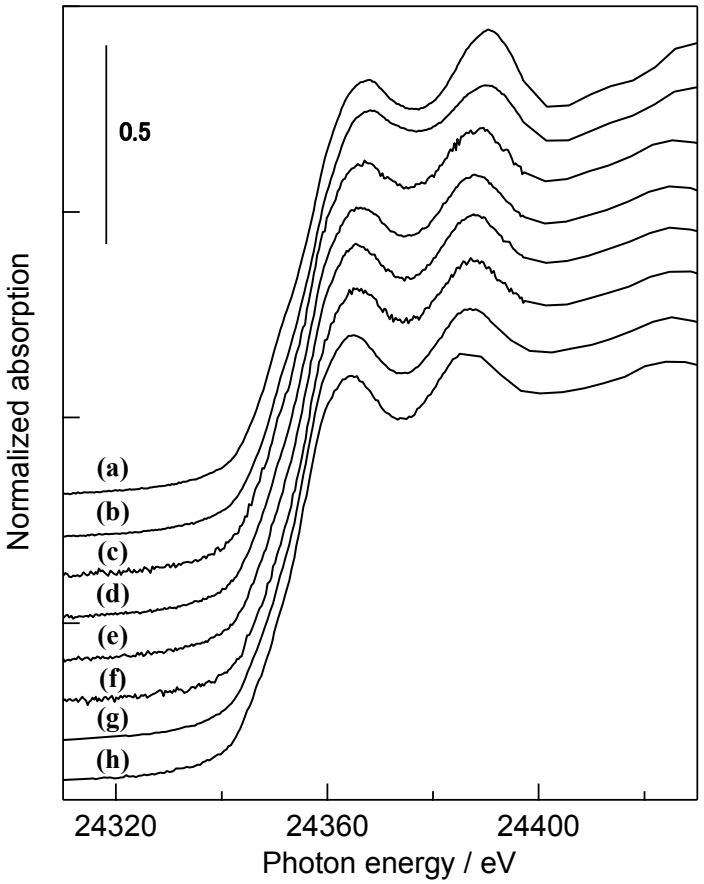

Figure 8. Pd K-edge XANES spectra of (a) Pd foil and SiO_2-supported PdAu alloy catalysts with different Pd/Au ratio (b)Pd only, (c)3Pd1Au, (d)1Pd1Au, (e)1Pd2Au, (f)1Pd3Au, (g)1Pd5Au, (h) 1Pd10Au

We also performed curve-fitting analyses of Au-L3 and Pd-K edge EXAFS spectra of supported Pd–Au catalysts.[82] Figure 9 shows the relationship between the coordination number of supported Pd–Au alloy catalysts and the Au content in Pd–Au alloy catalysts as estimated by atomic absorption spectroscopy. The coordination numbers of Pd-Pd and Au-Pd gradually decreased with a decrease in the Pd/Au atomic ratio in the Pd–Au alloy NPs. In contrast, the coordination numbers of Pd-Au and Au-Au increased with a decrease in the Pd/Au ratio. Based on these results, possible structures of Pd–Au alloys with different Pd/Au ratios are illustrated in Scheme 1. The configuration of Pd and Au atoms on the surface of Pd–Au alloy NPs varies with changes in the Pd/Au ratio, and a number of isolated single Pd atoms surrounded by Au atoms are present in Pd–Au alloys with a low Pd/Au atomic ratio. For supported Pd–Au catalysts with Pd/Au ratios of 1/3 and 1/5, which showed high catalytic activity in the hydrosilylation of α,β-unsaturated ketone and internal alkynes, the coordination numbers of Pd-Pd and Au-Pd linkages are quite small (< 1.0). These results suggest that Pd–Au alloy with isolated single Pd atoms surrounded by Au atoms showed high activity in hydrosilylation. Moreover, Figure 10 shows the relationship between the ratio of Pd-Au/Pd-Pd coordination numbers and the turnover frequency (TOF: product mmol• Pd $mmol^{-1}$• h^{-1}) based on a Pd atom toward the alkyne hydrosilylation of $PdAu/SiO_2$ catalysts with various Pd/Au ratios. The ratio of Pd-Au/Pd-Pd coordination numbers reflects the degree of isolation of Pd atoms in alloy particles and a high value indicates the presence of a large number of isolated single Pd atoms surrounded by Au atoms on the surface of Pd–Au alloy NPs. The close correlation between these two factors clearly suggests that such single Pd atoms in Pd–Au NPs act as the main active site for the efficient and selective hydrosilylation of α,β-unsaturated ketones and internal alkynes, and the activity of each catalyst completely depends on the number of isolated single Pd atoms on the surface of Pd–Au NPs. Similar catalysis have been reported by Zhang and coworkers, in which isolated

single Pd atom in Au NPs worked as main active site for Ullmann coupling of aryl chlorides.[61]

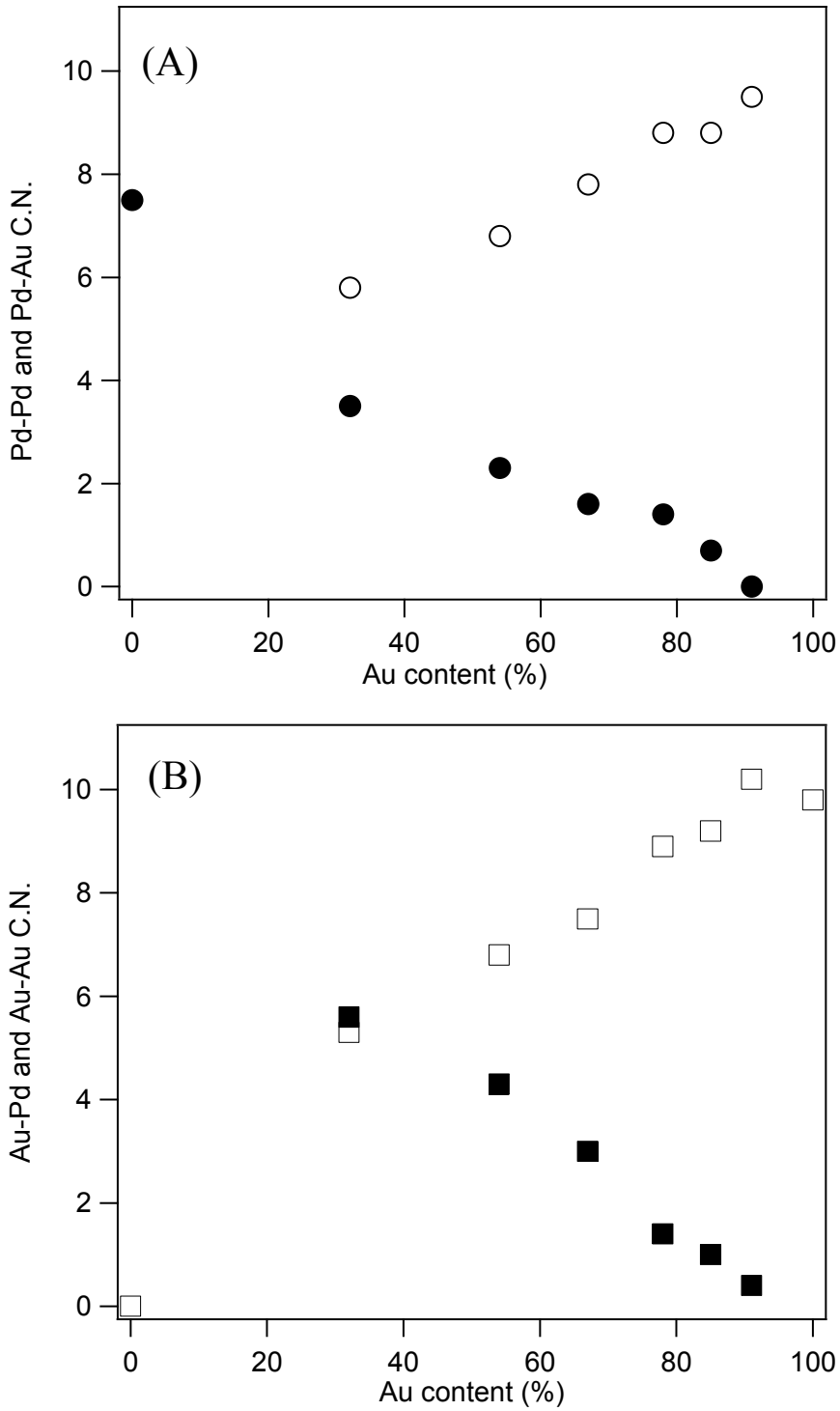

Figure 9. Relationship between Au content in $PdAu/SiO_2$ and (A) Pd-Pd(●) and Pd-Au(○) and (B)Au-Pd(■) and Au-Au(□) coordination numbers estimated by Pd K- and Au L_3-edge XAFS analysis.

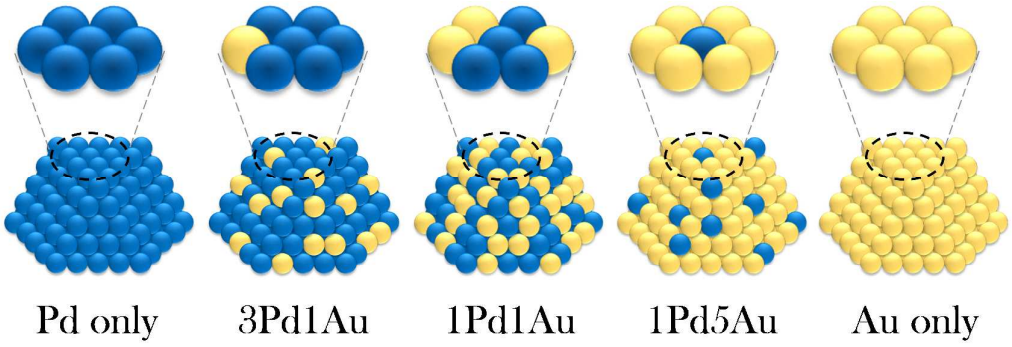

Scheme 1. Proposed structures of Pd-Au alloy NPs

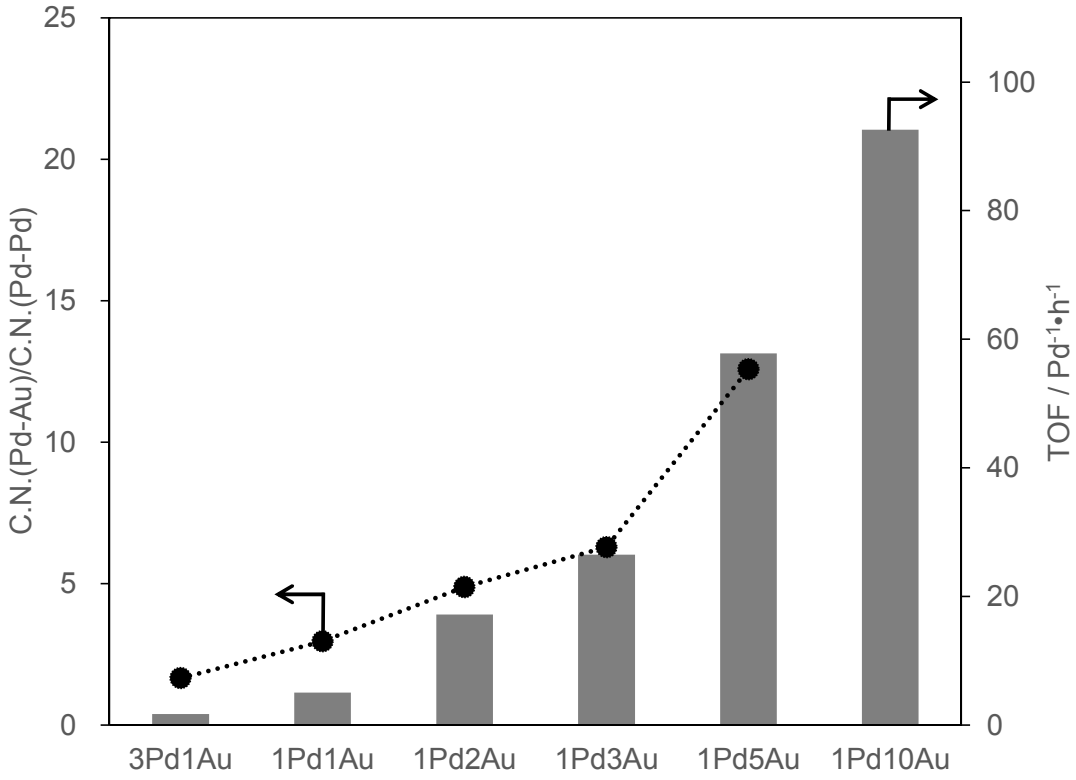

Figure 10. Relationship between Pd-Au/Pd-Pd coordination numbers ratio with the TOF based on a Pd in $PdAu/SiO_2$ toward alkyne hydrosilylation at 40 °C.

In the present catalytic system, the supports also remarkably affected the catalytic activity for hydrosilylation,[83] and catalysts supported on acidic metal oxides such as Nb_2O_5 and TiO_2 showed activities superior to those supported on neutral or basic metal oxides. In the XANES and EXAFS spectra of Nb_2O_5-supported Pd–Au catalysts, the overall trend was similar to those of SiO_2-supported catalysts (Figures S10-S14 and Table S4). The exact role of the support in the enhanced catalytic activity is not fully understood. It is likely that the Lewis acidic property of the support decreases the electron density of Pd–Au alloy NPs, which accelerates the reductive elimination of intermediate **C** to realize the rapid formation of products **3**. Likewise, the isolated Pd species on the surface of PdAu alloy NPs with low Pd/Au ratio become electron deficient due to high electronegativity of Au atom, which may accelerate the catalytic reaction. Detailed kinetic and computational investigations on the effect of alloying Pd and Au and their supports are currently underway in our laboratory.

3. Conclusion

We developed highly active supported Pd–Au alloy catalysts for the hydrosilylation of α,β-unsaturated ketones and alkynes. While supported monometallic Au or Pd NP catalysts were totally ineffective, the reactions with Pd–Au alloy catalysts proceeded efficiently under mild reaction conditions to give the corresponding silyl enol ethers and vinylsilanes in high yields with excellent selectivities. Particularly, supported Pd–Au alloy catalysts with low Pd/Au atomic ratios showed high activity. The detailed characterization of supported Pd–Au alloy catalysts by a series of spectroscopic techniques revealed the formation of a random Pd–Au alloy with a uniform size of around 3 nm. Furthermore, the electronic state and configuration of Au and Pd atoms in Pd–Au alloy NPs could be varied by changing the Pd/Au atomic ratio. For catalysts with a low Pd/Au atomic ratio, isolated single Pd atoms were present in the random Pd–Au alloy, which acted as the main catalytic active site for the efficient hydrosilylation of unsaturated compounds under mild reaction conditions. Further applications of supported Pd–Au alloy catalysts in other synthetic reactions as well as elucidation of the effect of alloying Pd and Au and their supports are currently under investigation in our laboratory.

4. Experimental

4.1. Materials

$PdCl_2$ and $HAuCl_4 \cdot 3H_2O$ were purchased from FURUYA METAL Co. Ltd and Wako Chemicals, respectively. Al_2O_3 (Sumitomo Chemical Co., Ltd, AKP-G015; JRC-ALO-8 equivalent), TiO_2 (JRC-TIO-4), ZrO_2 (JRC-ZRO-3), CeO_2 (JRC-CEO-2), were obtained from the Catalysis Society of Japan. SiO_2 (CARiACT Q-10) and $Nb_2O_5 \cdot nH_2O$ were kindly provided by Fuji Silysia Chemical Ltd and CBMM, respectively. Nb_2O_5 was obtained by the calcination of $Nb_2O_5 \cdot nH_2O$ at 550 ^oC for 3 h under air flow. Poly(*N*-vinylpyrrolidone) (PVP, K30) was purchased from Wako Chemicals. $Au(en)_2Cl_3$ (en = ethylenediamine) was synthesized by the method reported in the literature.[84] Other chemicals were of analytical grade and used as received without further purification.

4.2. Preparation of supported catalysts

4.2.1. Preparation of supported Pd–Au alloy NPs catalysts by a sol-immobilization method

Supported Pd–Au alloy catalysts were prepared through a colloid immobilization method.[85] To an aqueous solution (40 mL) containing the desired molar ratio of $PdCl_2$ to $HAuCl_4 \cdot 3H_2O$ was added PVP (K30, 36 mg), and the solution was cooled to 273 K with an ice bath. Subsequently, 0.1 M aqueous solution of $NaBH_4$ (8.0 mL, $NaBH_4$/metal (mol/mol) = 5) was added rapidly under vigorous stirring. After 0.5 h of colloid generation, 0.97 g of inorganic support was added to the colloidal solution, which was acidified to pH 1–3 with 0.1 M hydrochloric acid. After vigorous stirring overnight at room temperature, the resulting gray powder was separated from the suspension by centrifugation, thoroughly washed with distilled water, and dried overnight at 80 ^oC. The obtained catalysts were denoted xPdyAu/support, where x and y indicate the molar ratio of Pd to Au. The total loading amount of metal was set at 3wt%. Supported monometallic Pd and Rh NPs catalysts were

prepared by a method similar to that used for supported Pd–Au catalysts, but with the use of $PdCl_2$ or $RhCl_3$ as a metal precursor.

4.2.2. Preparation of Au/SiO_2 and Au/Nb_2O_5 catalysts by a deposition-precipitation method

SiO_2-supported Au catalysts were prepared by a deposition-precipitation method with the use of $Au(en)_2Cl_3$ as a Au precursor.[84] The pH value of an aqueous solution containing 50 mg of $Au(en)_2Cl_3$ was adjusted to 10 by 1M NaOH solution. After 0.97 g of SiO_2 or Nb_2O_5 was added to the solution, the pH value was re-adjusted to 10 with 1M NaOH solution. The suspension was stirred at 343 K for 2 h, separated by centrifugation, and then washed three times with methanol. The resulting powder was dried in vacuo at 343 K for 5 h. Prior to their use in catalytic reactions, the catalysts were reduced in a hydrogen atmosphere at 423 K for 1 h and calcined in air at 773 K for 1h. The total loading amount of metal was set at 3wt%.

4.2.3. Preparation of Nb_2O_5-supported metal NPs catalysts prepared by an impregnation method

Nb_2O_5-supported monometallic (Pt or Ru) catalysts were prepared by an impregnation method with the use of H_2PtCl_6 or $RuCl_3$ as a metal precursor. Nb_2O_5 was added to an aqueous solution of the metal precursor, and the suspension was stirred at 353 K for 2 h. After the evaporation of water, the resulting powder was calcined in air at 673 K for 1 h, and then reduced in a hydrogen atmosphere at 673 K for 1 h to give Nb_2O_5-supported Pt and Ru catalysts. The total loading amount of metal was set at 3wt%.

4.3. Physical and analytical measurements

The products of the catalytic runs were analyzed by GC-MS (Shimadzu GCMS-QP2010, CBP-10 capillary column, i.d. 0.25 mm, length 30 m, 50–250 ^oC) and gas chromatography

(Shimadzu GC-2014, CBP-10 capillary column, i.d. 0.25 mm, length 30 m, 50–250 ^{o}C). NMR spectra were recorded on a JMN-ECS400 (FT, 400 MHz (^{1}H), 100 MHz (^{13}C)) instrument. Chemical shifts (δ) of ^{1}H and ^{13}C{^{1}H} NMR spectra are referenced to $SiMe_4$.

The supported catalysts were analyzed by nitrogen gas adsorption, TEM, XRD, XPS and XAFS. High angle annular dark field-scanning transmission electron microscope (HADDF-STEM) images were recorded using a JEOL JEM-3200FS transmission electron microscope. The samples were prepared by depositing drops of ethanol suspensions containing small amounts of the powders onto carbon-coated copper grids (JEOL Ltd.) followed by evaporation of the ethanol in air. X-ray powder diffraction analyses were performed using Cu $K\alpha$ radiation and a one-dimensional X-ray detector (XRD: SmartLab, RIGAKU). The samples were scanned from 2θ=36° to 42° at a scanning rate of 0.067 s^{-1} and a resolution of 0.01°. X-ray photoelectron spectroscopy (XPS) of the catalysts was performed using a JPS-9010 MX instrument. The spectra were measured using MgK_α radiation (15 kV, 400 W) in a chamber at a base pressure of ~10^{-7} Pa. All spectra were calibrated using C_{1s} (284.6 eV) as a reference. The Brunauer–Emmett–Teller (BET) specific surface area was estimated from N_2 isotherms obtained using a BELSORP-mini II (BEL Japan, Osaka, Japan) at 77 K. The analyzed samples were evacuated at 573 K for 2 h prior to the measurement. Pd K-edge and Au L3-edge XAFS measurements were performed at the BL01B1 beam line at SPring-8 operated at 8 GeV using a Si(311) two-crystal monochromator. XAFS spectra were obtained at room temperature. XAFS data were processed to isolate EXAFS spectra from the background using Athena software. Replicate scans were averaged to increase the signal-to-noise ratios. The resulting EXAFS spectra (k space) were Fourier transformed (Pd K, k range/10 nm^{-1} 3.0 < k< 15.0; Au L_3, k range/10 nm^{-1} 3.0 < k< 15.0) and fitted in R space (Pd K, ΔR = 1.8− 3.2 /10^{-1} nm; Au L_3, ΔR= 1.8−3.3/10^{-1} nm) using Artemis software. Pd−Pd, Pd−Au, Au−Au, and Au−Pd single scattering paths were generated using FEFF. Amplitude reduction factors, for the Pd−Pd and Au−Au paths, S_0^2 = 0.87 and 0.82, respectively, were

determined by fitting the EXAFS of Pd and Au foils, respectively. The reported EXAFS parameters C.N. (coordination number), *R* (interatomic distance), σ^2 (Debye− Waller factor), and ΔE_0 (inner potential shift) are based on simultaneous fits of k^3 -weighted spectra.[86, 87] XANES were analyzed using the REX2000 version 2.5 (Rigaku). The actual contents of palladium and gold species immobilized on the supports were determined by atomic emission spectroscopic analysis with a SHIMADZU AA-6200.

4.4 General procedure for catalytic hydrosilylation

A typical reaction procedure is as follows: α,β-unsaturated ketones (1.0 mmol) and CH_3CN (2.0 mL) were added to a Schlenk tube containing the supported Pd–Au catalyst (2 mol% as metal) under an Ar atmosphere. The amount of Pd–Au catalyst used in the catalytic reaction was calculated based on the total amount of the two metals. The reaction was initiated by the injection of 1.0 mmol of hydrosilane at room temperature. The progress of the reaction was monitored by thin layer chromatography (TLC) and GC analysis. After the ketones were completely comsumed, the products were quantified by GC using biphenyl as an internal standard. For isolation of the products, the solid catalyst was removed by passing the mixture through a 0.45 μm polytetrafluoroethylene (PTFE) filter (Millipore Millex LH) The remaining solution was concentrated under reduced pressure and purified through silica gel column chromatography (hexane : NEt_3 = 100 : 1, v/v) to give the product. The isomeric ratio and *E*/*Z* configuration of the products were determined by ^{1}H NMR and NOESY, respectively.

4.5 Characterization data of the products

Products **3a**[75], **3l**[88], **3m**[75], **3n**[75], **3o**[62] and **3p**[62] are known compounds and were identified by comparison of their NMR features with the respective reported data.

(*Z*)-triethyl((3-(4-methoxyphenyl)-1-phenylprop-1-en-1-yl)oxy)silane (**3b**)

Colorless liquid; ^{1}H NMR (400 MHz, $CDCl_3$, ppm) δ 7.50-7.46 (m, 2H), 7.32-7.22 (m, 3H), 7.19-7.15 (m, 2H), 6.86-6.80 (m, 2H), 5.29 (t, *J* = 7.2 Hz, 1H), 3.78(s, 3H), 3.52 (d, *J* = 7.2 Hz, 2H), 0.94 (t, *J* = 8.0 Hz, 9H), 0.63 (q, *J* = 8.0 Hz, 6H). ^{13}C NMR (100 MHz, $CDCl_3$, ppm) δ 152.8, 144.9, 134.4, 128.6, 124.3, 123.0, 122.6, 120.6, 108.8, 105.2, 50.3, 1.8, 0.4. HRMS (FAB) m/z $[M]^+$ calculated for $C_{22}H_{30}O_2Si$ 354.2015, found 354.2011.

(*Z*)-triethyl((1-phenyl-3-(p-tolyl)prop-1-en-1-yl)oxy)silane (**3c**)

Colorless liquid; ^{1}H NMR (400 MHz, $CDCl_3$, ppm) δ 7.53-7.43 (m, 2H), 7.32-7.21 (m, 3H), 7.12 (q, *J* = 10.7 Hz, 4H), 5.30 (t, *J* = 7.2 Hz, 1H), 3.55 (d, *J* = 7.2 Hz, 2H), 2.32 (s, 3H), 0.94 (t, *J* = 8.0 Hz, 9H), 0.64 (q, *J* = 8.0 Hz, 6H). ^{13}C NMR (100 MHz, $CDCl_3$, ppm) δ 149.9, 139.4, 138.5, 135.2, 129.0, 128.3, 127.9, 127.5, 125.6, 110.0, 31.8, 21.0, 6.7, 5.4. HRMS (FAB) m/z $[M]^+$ calculated for $C_{22}H_{30}OSi$ 338.2066, found. 338.2064.

(*Z*)-triethyl((3-(4-fluorophenyl)-1-phenylprop-1-en-1-yl)oxy)silane (**3d**)

Colorless liquid; ^{1}H NMR (400 MHz, $CDCl_3$, ppm) δ 7.50-7.45 (m, 2H), 7.32-7.17 (m, 5H), 6.96 (t, *J* = 8.8 Hz, 2H), 5.27 (t, *J* = 7.2 Hz, 1H), 3.55 (d, *J* = 7.2 Hz, 2H), 0.94 (t, *J* = 8.0 Hz, 9H), 0.63 (q, *J* = 8.0 Hz, 6H). ^{13}C NMR (100 MHz, $CDCl_3$, ppm) δ 162.5 (d, J_{C-F} = 241 Hz), 145.4, 134.4, 132.2 (d, J_{C-F} = 3.0 Hz), 124.7 (d, J_{C-F} = 7.0 Hz), 123.1, 122.8, 120.8, 110.1 (d, J_{C-F} = 21 Hz), 104.6, 26.5, 1.8, 0.5. HRMS (FAB) m/z $[M]^+$ calculated for $C_{21}H_{27}FOSi$ 342.1815, found. 342.1806.

(*Z*)-((3-(4-chlorophenyl)-1-phenylprop-1-en-1-yl)oxy)triethylsilane (**3e**)

Colorless liquid; ^{1}H NMR (400 MHz, $CDCl_3$, ppm) δ 7.50-7.45 (m, 2H), 7.32-7.22 (m, 5H), 7.20-7.16 (m, 2H), 5.25 (t, *J* = 7.2 Hz, 1H), 3.54 (d, *J* = 7.2 Hz, 2H), 0.93 (t, *J* = 8.0 Hz, 9H), 0.62 (q, *J* = 8.0 Hz, 6H). ^{13}C NMR (100 MHz, $CDCl_3$, ppm) δ 150.6, 140.0, 139.2, 131.5,

129.7, 128.4, 128.0, 127.8, 125.7, 109.0, 31.5, 6.7, 5.4. HRMS (FAB) m/z $[M]^+$ calculated for $C_{21}H_{27}ClOSi$ 358.1520, found. 358.1504.

(*Z*)-triethyl((1-phenyl-3-(4-(trifluoromethyl)phenyl)prop-1-en-1-yl)oxy)silane (**3f**)

Colorless liquid; ^1H NMR (400 MHz, $CDCl_3$, ppm) δ 7.53 (d, *J* = 8.0 Hz, 2H), 7.49-7.45 (m, 2H), 7.36 (d, *J* = 8.0 Hz, 2H), 7.33-7.22 (m, 3H), 5.26 (t, *J* = 7.2 Hz, 1H), 3.63 (d, *J* = 7.2 Hz, 2H), 0.94 (t, *J* = 8.0 Hz, 9H), 0.63 (q, *J* = 8.0 Hz, 6H). ^{13}C NMR (100 MHz, $CDCl_3$, ppm) δ 151.0, 145.7, 139.1, 128.6, 128.3, 128.0, 125.7, 125.2 (d, J_{C-F} = 3.6 Hz), 123.0, 108.3, 32.0, 6.7, 5.4. HRMS (FAB) m/z $[M]^+$ calculated for $C_{22}H_{27}F_3OSi$ 392.1783, found. 392.1773.

(*Z*)-triethyl((1-(4-methoxyphenyl)-3-phenylprop-1-en-1-yl)oxy)silane (**3g**)

Colorless liquid; ^1H NMR (400 MHz, $CDCl_3$, ppm) δ 7.43-7.38 (m, 2H), 7.32-7.14 (m, 5H), 6.85-6.79 (m, 2H), 5.20 (t, *J* = 7.2 Hz, 1H), 3.80 (s, 3H), 3.57 (d, *J* = 7.2 Hz, 2H), 0.95 (t, *J* = 8.0 Hz, 9H), 0.63 (q, *J* = 8.0 Hz, 6H). ^{13}C NMR (100 MHz, $CDCl_3$, ppm) δ 159.2, 149.8, 141.7, 132.1, 128.4, 128.3, 126.9, 125.7, 113.3, 108.2, 55.2, 32.2, 6.8, 5.4. HRMS (FAB) m/z $[M]^+$ calculated for $C_{22}H_{30}O_2Si$ 354.2015, found. 354.2030.

(*Z*)-triethyl((3-phenyl-1-(p-tolyl)prop-1-en-1-yl)oxy)silane (**3h**)

Colorless liquid; ^1H NMR (400 MHz, $CDCl_3$, ppm) δ 7.39-7.35 (m, 2H), 7.32-7.14 (m, 5H), 7.12-7.07 (m, 2H), 5.27 (t, *J* = 7.2 Hz, 1H), 3.58 (d, *J* = 7.2 Hz, 2H), 2.33 (s, 3H), 0.95 (t, *J* = 8.0 Hz, 9H), 0.63 (q, *J* = 8.0 Hz, 6H). ^{13}C NMR (100 MHz, $CDCl_3$, ppm) δ 150.1, 141.7, 137.3, 136.5, 128.6, 128.4, 128.3, 125.7, 125.6, 108.9, 32.2, 6.8, 5.4. HRMS (FAB) m/z $[M]^+$ calculated for $C_{22}H_{30}OSi$ 338.2066, found. 338.2067.

(*Z*)-((1-(4-chlorophenyl)-3-phenylprop-1-en-1-yl)oxy)triethylsilane (**3i**)

Colorless liquid; ^1H NMR (400 MHz, $CDCl_3$, ppm) δ 7.43-7.39 (m, 2H), 7.33-7.21 (m, 6H),

7.21-7.16 (m, 1H), 5.30 (t, J = 7.6 Hz, 1H), 3.57 (d, J = 7.6 Hz, 2H), 1.00 (t, J = 8.0 Hz, 9H), 0.63 (q, J = 8.0 Hz, 6H). ^{13}C NMR (100 MHz, $CDCl_3$, ppm) δ 149.1, 141.2, 137.9, 133.3, 128.4, 128.4, 128.2, 126.9, 125.9, 110.3, 32.3, 6.7, 5.4. HRMS (FAB) m/z $[M]^+$ calculated for $C_{21}H_{27}ClOSi$ 358.1520, found. 358.1504.

(*Z*)-triethyl((1-(furan-2-yl)-3-phenylprop-1-en-1-yl)oxy)silane (**3j**)

Colorless liquid; ^{1}H NMR (400 MHz, $CDCl_3$, ppm) δ 7.30-7.21 (m, 5H), 7.21-7.15 (m, 1H), 6.37-6.31 (m, 2H), 5.48 (t, J = 7.2 Hz, 1H), 3.55 (d, J = 7.2 Hz, 2H), 1.00 (t, J = 8.0 Hz, 9H), 0.74 (q, J = 8.0 Hz, 6H). ^{13}C NMR (100 MHz, $CDCl_3$, ppm) δ 152.5, 141.5, 141.5, 128.4, 128.4, 125.9, 110.9, 108.2, 105.8, 105.8, 31.5, 6.7, 5.3. HRMS (FAB) m/z $[M+H]^+$ calculated for $C_{19}H_{27}O_2Si$ 315.1780, found. 315.1770.

(*Z*)-triethyl((1-(4-methoxyphenyl)hex-1-en-1-yl)oxy)silane (**3k**)

Colorless liquid; ^{1}H NMR (400 MHz, $CDCl_3$, ppm) δ 7.40-7.33 (m, 2H), 6.84-6.79 (m, 2H), 5.02 (t, J = 7.2 Hz, 1H), 3.80 (s, 3H), 2.24-2.15 (m, 2H), 1.44-1.30 (m, 4H), 0.96-0.90 (m, 12H), 0.61 (q, J = 8.0 Hz, 6H). ^{13}C NMR (100 MHz, $CDCl_3$, ppm) δ 158.9, 148.9, 132.5, 126.7, 113.2, 110.0, 55.2, 32.0, 25.8, 22.6, 14.0, 6.7, 5.3. HRMS (FAB) m/z $[M]^+$ calculated for $C_{19}H_{32}O_2Si$ 320.2172, found. 320.2182.

(*Z*)-tributyl((1,3-diphenylprop-1-en-1-yl)oxy)silane (**3q**)

Colorless liquid; ^{1}H NMR (400 MHz, $CDCl_3$, ppm) δ 7.49-7.45 (m, 2H), 7.33-7.15 (m, 8H), 5.30 (t, J = 8 Hz, 1H), 3.58 (d, J = 8 Hz, 2H), 1.34 (m, 13H), 0.87-0.80 (m, 8H), 0.65-0.56 (m, 6H). ^{13}C NMR (100 MHz, $CDCl_3$, ppm) δ 150.3, 141.6, 139.5, 128.4, 128.3, 127.9, 127.6, 125.8, 109.6, 32.3, 26.6, 25.2, 14.2, 13.9, 13.7. HRMS (FAB) m/z $[M+H]^+$ calculated for $C_{27}H_{41}OSi$ 409.2927, found. 409.2947.

(*Z*)-*tert*-butyl((1,3-diphenylprop-1-en-1-yl)oxy)dimethylsilane (**3r**)

Colorless liquid; ^{1}H NMR (400 MHz, $CDCl_3$, ppm) δ 7.51-7.46 (m, 2H), 7.33-7.17 (m, 8H), 5.31 (t, *J* = 7.2 Hz, 1H), 3.60 (d, *J* = 7.2 Hz, 2H), 1.03 (s, 9H), 0.01 (s, 6H). ^{13}C NMR (100 MHz, $CDCl_3$, ppm) δ 149.9, 141.5, 139.5, 128.4, 128.3, 127.9, 127.6, 126.0, 125.8, 110.3, 32.3, 25.9, 18.4, -3.9. HRMS (FAB) m/z $[M]^+$ calculated for $C_{21}H_{28}OSi$ 324.1909, found. 324.1919.

(*Z*)-triethoxy(1,3-diphenylprop-1-en-1-yl)silane (**3s**)

Colorless liquid; ^{1}H NMR (400 MHz, $CDCl_3$, ppm) δ 7.58-7.56 (m, 2H), 7.33-7.15 (m, 8H), 5.46 (t, *J* = 7.2 Hz, 1H) , 3.83 (q, *J* = 7.2 Hz, 6H), 3.67 (d, *J* = 7.2 Hz, 2H), 1.17 (t, *J* = 7.2 Hz, 9H). ^{13}C NMR (100 MHz, $CDCl_3$, ppm) δ147.7, 141.4, 137,9, 128.5, 128.3, 128.0, 127.6, 125.8, 125.4, 110.4, 59.5, 32.1, 18.0 HRMS (FAB) m/z $[M]^+$ calculated for $C_{21}H_{28}O_4Si$ 372.1757, found 372.1749.

Acknowledgement

This study was supported in part by the Program for Element Strategy Initiative for Catalysts & Batteries (ESICB), Platform for Technology and Industry and a Grant-in-Aid for Young Scientists (B) (No. 26820353), commissioned by the Ministry of Education, Culture, Sports, Science and Technology (MEXT) of Japan. The XAFS experiment at SPring–8 was carried out under the approval (proposal No. 2015B1478) of Japan Synchrotron Radiation Research Institute (JASRI). We wish to thank Mr. Eichi Watanabe of Tokyo Metropolitan University for providing valuable technical support during the HAADF-TEM observations.

Supporting Information Available: Optimization of catalysts and reaction condition for alkyne hydrosilylation, characterization of supported PdAu catalysts, ^{1}H NMR, ^{13}C NMR and NOESY spectra of the products. This material is available free of charge via the Internet at http://pubs.acs.org.

References

(1) Hiyama, T.; Kusumoto, T. In *Comprehensive Organic Synthesis* Vol. *8*; Trost, B. M.; Fleming, I. Ed.; Pergamon Press: Oxford, 1991.

(2) Marciniec, B.; Guliński, J.; Urbaniac, W.; Kornetka, Z. W. In *Comprehensive Handbook on Hydrosilylation*; Marciniec, B. Ed.; Pergamon Press: Oxford, 1992.

(3) Marciniec, B.; Maciejewski, H.; Pietraszuk, C.; Pawluć, P. In *Hydrosilylation: A Comprehensive Review on Recent Advances*; Marciniec, B. Ed.; Springer: Berlin, 2009.

(4) Corey, J. Y. *Chem. Rev.* **1999**, *99*, 175–292.

(5) Trost, B. M.; Ball, Z. T. *Synthesis* **2005**, 853–887.

(6) Marciniec, B. *Coord. Chem. Rev.* **2005**, *249*, 2374–2390.

(7) Díez-González S.; Nolan, S. P. *Acc. Chem. Rev.* **2008**, *41*, 349–358.

(8) Corey, J. Y. *Chem. Rev.* **2011**, *111* 863−1071.

(9) Corey, J. Y. *Chem. Rev.* **2016**, **DOI:** 10.1021/acs.chemrev.5b00559 and references cited therein.

(10) Anastas, P. T.; Warner, J. In *Green Chemistry: Theory and Practice*; Oxford University Press: New York, 1998.

(11) Sheldon, R. A.; Downing, R. S. *Appl. Catal. A: General* **1999**, *189*, 163−183.

(12) Trost, B. M. *Acc. Chem. Res.* **2002**, *35*, 695−705.

(13) Laszlo, P. *Acc. Chem. Res.* **1986**, *19*, 121−127.

(14) Izumi, Y.; Onaka, M. *Adv. Catal.* **1992**, *38*, 245−282.

(15) Clark, J. H.; Macquarrie, D. J. *Chem. Soc. Rev.* **1996**, *25*, 303−310.

(16) Sels, B. F.; De Vos, D. E.; Jacobs, P. A. *Catal. Rev. Sci. Eng.* **2001**, *43*, 443−488.

(17) Nishimura, T.; Uemura, S. *Synlett* **2004**, 201.

(18) Kannan, S. *Catal. Surv. Asia* **2006**, *10*, 117−137.

(19) Kaneda, K. *Synlett* **2007**, 999−1015.

(20) Yin, L.; Liebscher, J. *Chem. Rev.* **2007**, *107*, 133−173.

(21) Astruc, D. *Nanoparticles and Catalysis*; Astruc, D. Ed.; Wiley-VCH: Weinheim, Germany, 2007.

(22) Kaneda, K.; Ebitani, K.; Mizugaki, T.; Mori, K. *Bull. Chem. Soc. Jpn.* **2006**, *79*, 981−1016.

(23) Nishimura, S.; Ebitani, K. *ChemCatChem* **2016**, *8*, 2303−2316.

(24) Polizzi C.; Caporusso, A. M.; Vitulli, G.; Salvadori, P.; Pasero, M. *J. Mol. Catal.* **1994**, *91*, 83−90.

(25) Chauhan, M.; Hauck, B. J.; Keller, L. P.; Boudjouk, P. *J. Organomet. Chem.* **2002**, *645*, 1−13.

(26) Alonso, F.; Buitrago, R.; Moglie, Y.; Ruiz-Martinez, J.; Sepulveda-Escribano, A.; Yus, M. *J. Organomet. Chem.* **2011**, *696*, 368−372.

(27) Cano, R.; Yus, M.; Ramon, D. J. *ACS. Catal.* **2012**, *2*, 1070−1078.

(28) Ciriminna, R.; Pandarus, V.; Gingras, G.; Beland, F.; Pagliaro, M. *ACS. Sustainable Chem. Eng.* **2013**, *1*, 249−253.

(29) Benohoud, M.; Tuokko, S.; Pihko, P. M. *Chem. Eur. J.* **2011**, *17,* 8404−8413.

(30) Planellas, M.; Guo, W.; Alonso, F.; Yus, M.; Shafir, A.; Pleixats, R.; Parella, T. *Adv. Synth. Catal.* **2014**, *356*, 179−188.

(31) Yamada, Y. M. A.; Yuyama, Y.; Sato, T.; Fujikawa, S.; Uozumi, Y. *Angew. Chem. Int. Ed.* **2014**, *53,* 127−131.

(32) Reddy, C. B.; Shil, A. K.; Guha, N. R.; Sharma, D.; Das, P. *Catal. Lett.* **2014**, *144*, 1530−1536.

(33) Solomonsz, W. A.; Rance, G. A.; Suyetin, M.; La Torre, A.; Bichoutskaia, E.; Khlobystov, A. N. *Chem. Eur. J.* **2012**, *18,* 13180−13187.

(34) Guo, W.; Pleixats, R.; Shafir, A.; Parella, T. *Adv. Synth. Catal.* **2015**, *357*, 89−99.

(35) Blandez, J. F.; Esteve-Adell, I.; Primoa, A.; Alvaroa, M.; García, H. *J. Mol. Catal. A: General* **2016**, *412*, 13–19.

(36) Corma, A.; González-Arellano, C.; Iglesias, M.; Sánchez, F. *Angew. Chem. Int. Ed.* **2007**, *46,* 7820–7822.

(37) Psyllaki, A.; Lykakis, I.; Stratakis, M. *Tetrahedron* **2012**, *68,* 8724–8731.

(38) Gryparis, C.; Kidonakis, M.; Stratakis, M. *Org. Lett.* **2013**, *15,* 6038–6041.

(39) Ishikawa, Y.; Yamamoto, Y.; Asao, N. *Catal. Sci. Technol.* **2013**, *3,* 2902–2905.

(40) Kidonakis, M.; Stratakis, M. *ACS. Catal.* **2015**, *5,* 4538–4541.

(41) Toshima, N.; Yonezawa, T. *New J. Chem.* **1998**, 1179–1201.

(42) Bracey, C. L.; Ellis, P. R.; Hutchings, G. J. *Chem. Soc. Rev.* **2009**, *38,* 2231–2243.

(43) Sankar, M.; Dimitratos, N.; Miedziak, P. J.; Wells, P. P.; Kielye, C. J.; Hutchings, G. J. *Chem. Soc. Rev.* **2012**, *41,* 8099–8139.

(44) Francesco, I. N.; Fontaine-Vive, F.; Antoniotti, S. *ChemCatChem* **2014**, *6,* 2784–2791.

(45) Hutchings, G. J. *Chem. Commun.* **2008**, 1148–1164.

(46) Lopez-Sanchez, J. A.; Dimitratos, N.; Miedziak, P.; Ntainjua, E.; Edwards, J. K.; Morgan, D.; Carley, A. F.; Tiruvalam, R.; Kiely, C. J.; Hutchings, G. J. *Phys. Chem. Chem. Phys.* **2008**, *10*, 1921–1930.

(47) Pritchard, J.; Kesavan, L.; Piccinini, M.; He, Q.; Tiruvalam, R.; Dimitratos, N.; Lopez-Sanchez, J. A.; Carley, A. F.; Edwards, J. K.; Kiely, C. J.; Hutchings, G. J. *Langmuir* **2010**, *26*, 16568–16577.

(48) Kiely, C. J.; Hutchings, G. J. *Acc. Chem. Res.* **2013**, *46*, 1759–1772.

(49) Enache, D. I.; Edwards, J. K.; Landon, P.; Solsona-Espriu, B.; Carley, A. F.; Herzing, A. A.; Watanabe, M.; Kiely, C. J.; Knight, D. W.; Hutchings, G. J. *Science* **2006**, *311,* 362–365.

(50) Dimitratos, N.; Villa, A.; Wang, D.; Porta, F.; Su, D.; Prati, L. *J. Catal.* **2006**, *244,* 113–121.

(51) Hou, W.; Dehm, N. A.; Scott, R. W. J. *J. Catal.* **2008**, *253,* 22–27.

(52) Bianchi, C. L.; Canton, P.; Dimitratos, N.; Porta, F.; Prati, L. *Catal. Today* **2005**, *102-103,* 203–212.

(53) Wang, D.; Villa, A.; Porta, F.; Sua, D.; Prati, L. *Chem. Commun.* **2006**, 1956–1958.

(54) Marx, S.; Baiker, A. *J. Phys. Chem. C* **2009**, *113,* 6191–6201.

(55) Villa, A.; Dimitratos, N.; Chan-Thaw, C. E.; Hammond, C.; Prati, L.; Hutchings, G. J. *Acc. Chem. Res.* **2015**, *48*, 1403–1412.

(56) Kesavan, L.; Tiruvalam, R.; Ab Rahim, M. H.; bin Saiman, M. I.; Enache, D. I.; Jenkins, R. L.; Dimitratos, N.; Lopez-Sanchez, J. A.; Taylor, S. H.; Knight, D. W.; Kiely, C. J.; Hutchings, G. J. *Science* **2011**, *331,* 195–199.

(57) Long, J.; Liu, H.; Wu, S.; Liao, S.; Li, Y. *ACS. Catal.* **2013**, *3,* 647–654.

(58) Dhital, R. N.; Kamonsatikul, C.; Somsook, E.; Bobuatong, K.; Ehara, M.; Karanjit, S.; Sakurai, H. *J. Am. Chem. Soc.* **2012**, *134,* 20250–20253.

(59) Dhital, R. N.; Kamonsatikul, C.; Somsook, E.; Sakurai, H. *Catal. Sci. Technol.* **2013**, *3,* 3030–3035.

(60) Boekfa, B.; Pahl, E.; Gaston, N.; Sakurai, H.; Limtrakul, J.; Ehara, M. *J. Phys. Chem. C* **2014**, *118,* 22188–22196.

(61) Zhang, L.; Wang, A.; Miller, J. M.; Li, X.; Yang, X.; Wang, W.; Li, L.; Huang, Y.; Mou, C. Y.; Zhang, T. *ACS. Catal.* **2014**, *4,* 1546–1553.

(62) Chen, Q.; Tanaka, S.; Fujita, T.; Chen, L.; Minato, T.; Ishikawa, Y.; Chen, M.; Asao, N.; Yamamoto, Y.; Jin, T. *Chem. Commun.* **2014**, *50,* 3344–3346.

(63) Takale, B. S.; Bao, M.; Yamamoto, Y.; Almansour, A. I.; Arumugam, N.; Kumar, R. S. *Synlett* **2015**, *17,* 2355–2380.

(64) Ojima, I.; Nhonyanagi, M.; Kogure, T.; Kumagai, M.; Horiuchi, S; Nakatsugawa, K. *J. Organomet. Chem.* **1975**, *94*, 449–461.

(65) Johnson, C. R.; Raheja, R. K. *J. Org. Chem.* **1994**, *59,* 2287–2288.

(66) Zheng, G. Z.; Chan, T. H. *Organometallics* **1995**, *14,* 70–79.

(67) Lipshutz, b H.; Chrisman, W.; Noson, K.; Papa, P.; Sclafani, J. A.; Vivian, R. W.; Keith, J. M. *Tetrahedron* **2000**, *56,* 2779–2788.

(68) Mori, A.; Kato, T. *Synlett* **2002**, 1167–2380.

(69) Blackwell, J. M.; Morrison, D. J.; Piers, W. E. *Tetrahedron* **2002**, *58,* 8247–8254.

(70) Anada, M.; Tanaka, M.; Suzuki, K.; Nambu, H.; Hashimoto, S. *Chem. Pharm. Bull.* **2006**, *54,* 1622–1623.

(71) Imao, D.; Hayama, M.; Ishikawa, K.; Ohta, T.; Ito, Y. *Chem. Lett.* **2007**, *36,* 366–367.

(72) Sumida, Y.; Yorimitsu, H.; Oshima, K. *J. Org. Chem.* **2009**, *74,* 7986–7989.

(73) Dunsford, J. J.; Cavell, K. J.; Kariuki, B. *J. Organomet. Chem.* **2011**, *696,* 188–194.

(74) Huckaba, A. J.; Hollis, T. K.; Reilly, S. W. *Organometallics* **2013**, *32*, 6248–6256.

(75) Onodera, G.; Hachisuka, R.; Noguchi, T.; Miura, H.; Hashimoto, T.; Takeuchi, R. *Tetrahedron Lett.* **2014**, *55,* 310–313.

(76) Ikeda, N.; Konno, T. *J. Fluorine Chem.* **2015**, *173,* 69–76.

(77) The detailed data for the screening of catalysts are shown in Table S1 in the Supporting Information.

(78) The detailed data for the amount of metals as estimated by atomic absorption spectroscopy are shown in Table S2 in the Supporting Information.

(79) Denton, A. R.; Ashcroft, N. W. *Phys. Rev. A* **1991**, *43,* 3161–3164.

(80) Moulder, F.; Stickle, W. F.; Sobol, P. E.; Bomben, K. D. *Handbook of X-ray Photoelectron Spectroscopy*, Perkin-Elmer Co., Eden Prairie, USA, 1992.

(81) Lytle, F. W. *J. Catal.* **1976**, *43*, 376–379.

(82) The detailed curve-fitting results of Pd K- and Au L_3-edge EXAFS for SiO_2-supported Pd–Au catalysts are summarized in Table S3 in the Supporting Information.

(83) Au L_3-edge XANES spectra of supported Pd-Au catalysts on various metal oxides are shown in the Supporting Information.

(84) Venezia, A.M.; Liotta, L.F.; Pantaleo, G.; La Parola, V.; Deganello, G.; Beck, A.; Koppány, Zs.; Frey, K.; Horváth, D.; Guczi, L. *Appl. Catal. A: General* **2003**, *251*, 359–368.

(85) Brett, G. L.; He, Q.; Hammond, C.; Miedziak, P. J.; Dimitratos, N.; Sankar, M.; Herzing, A. A.; Conte, M.; Lopez-Sanchez, J. A.; Kiely, C. J.; Knight, D. W.; Taylor, S. H.; Hutchings, G. J. *Angew. Chem. Int. Ed.* **2011**, *50*, 10136–10139.

(86) Newville, M. *J. Synchrotron Radiat.* **2001**, *8*, 322−324.

(87) Rehr, J. J.; Albers, R. *Rev. Mod. Phys.* **2000**, *72*, 621−654.

(88) Campos, J.; Rubio, M.; Esqueda, A. C.; Carmona, E. *J. Labelled Compd. Radiopharm.* **2012**, *55*, 29–38.

Graphical Abstract